

Received February 9, 2022, accepted February 21, 2022, date of publication February 24, 2022, date of current version March 9, 2022.

Digital Object Identifier 10.1109/ACCESS.2022.3154418

# Adaptive Internal Model Control of SCR Denitration System Based on Multi-Objective Optimization

BO HU<sup>1</sup>, CHANG LIU<sup>1</sup>, YUAN YANG<sup>1</sup>, BIN WANG<sup>1</sup>, DAN CAI<sup>2</sup>, AND WEIFENG XU<sup>2</sup>

<sup>1</sup>Xi'an Thermal Power Research Institute Company Ltd., Xi'an 710000, China

<sup>2</sup>Nanjing NR Electric Company Ltd., Nanjing 210000, China

Corresponding author: Bo Hu (huboo@tpri.com.cn)

This work was supported by the Natural Science Foundation of Hebei Province, China, through the Research on data-driven modeling methods and optimization strategies for denitration systems of thermal power plants fund, under Grant E2018502111.

**ABSTRACT** Many thermal power plants use selective catalytic reduction (SCR) systems to complete flue gas denitration. The system has the characteristics of large inertia, large delay and nonlinearity. At the same time, it is difficult to use the controller under a single working condition to meet the control task of the system under the full working conditions. In order to solve the above control difficulties, This paper proposes a two-degree-of-freedom internal model control (2-DOF-IMC) method based on controller parameter adaptation and multi-model adaptation to realize the control of the full working conditions of the SCR system. First, the intelligent identification method based on Differential evolution quantum particle swarm optimization (DEQPSO) is used to obtain the sub-model of ammonia injection-SCR outlet Nitrogen Oxide (NO<sub>x</sub>) concentration in typical working conditions. A 2-DOF-IMC controller under each sub-model is established. Then, aiming at system set point tracking performance, anti-disturbance performance, and control energy consumption, the Pareto optimal solution of each controller is obtained by using the Non-dominated Sorting Genetic Algorithms-II (NSGA-II) algorithm based on chaotic mutation. Finally, the controller parameter adaptive strategy is designed based on the Takagi-Sugeno (T-S) fuzzy model, and the multi-model adaptive strategy is designed based on the recursive bayesian probability weighting. Through the dynamic performance test and the anti-disturbance performance test, it is verified that the 2-DOF-IMC based on controller parameter adaptation and multi-model adaptation has good control performance and adaptability to all working conditions. The method proposed in this paper combines the advantages of multi-parameter and multi-model strategies, further improves the control quality, and provides a new solution for the control of thermal power plant SCR system.


**INDEX TERMS** Selective catalytic reduction (SCR), two-degree-of-freedom internal model control (2-DOF-IMC), multi-objective optimization, parameter adaptation, multi-model adaptation.

## I. INTRODUCTION

The combustion of fossil fuels, especially in coal-fired power plants, is one of the main sources of NO<sub>x</sub> in the atmosphere [1]–[3]. Currently, thermal power plants have two ways to reduce NO<sub>x</sub> emissions. One is to reduce NO<sub>x</sub> emissions through staged combustion or improved combustion equipment during the combustion process. The other is to denitrify the combustion products. The specific method is to add denitrification equipment in the flue to treat the exhaust gas [4]. Among many flue gas denitration processes, Selective

catalytic reduction (SCR) is the most efficient and mature denitration method [5].

By analyzing the mechanism of SCR denitration, it can be known that the reaction process is more complicated. Especially under the background that thermal power units are deeply involved in power grid peak shaving, the non-linear characteristics of the SCR system in load changes are prominent. When the traditional PID controller is used to control the amount of ammonia injection, it is difficult to achieve the optimal amount of ammonia injection. Excessive amount of ammonia causes an increase in the escape rate of ammonia, which causes secondary pollution to the atmosphere and increases the cost of denitrification. The excessively low

The associate editor coordinating the review of this manuscript and approving it for publication was Vitor Monteiro .

amount of ammonia injection causes the tail gas  $NO_x$  content to exceed the standard, which fails to achieve the goal of energy saving and emission reduction [6].

In recent years, many experts and scholars have conducted a lot of theoretical research and exploration on the control of nonlinear systems [7]–[14]. Zhao Zhijia *et al.* proposed a fault-tolerant control based on an adaptive neural network for adaptive fault-tolerant boundary control of uncertain flexible systems [7]; Yu Xinbo *et al.* proposed an observer-based adaptive fuzzy output feedback control method to improve the control accuracy [11].

For SCR system control: Qin Tianmu *et al.* established an SCR system model using multi-scale kernel partial least squares, and combined this model with model predictive control for SCR system control [6]; Liu Guofu *et al.* established a multi-layer perception model of entrance  $NO_x$  prediction, which solved the problem of measurement lag, and used the model output as the feedforward of the SCR control strategy to improve the control effect [15]; Yang Tingting *et al.* added ultra-low emission and economic cost into the objective function of predictive control, constructed a multi-objective optimization control algorithm, and used genetic algorithm to obtain the control quantity to realize the optimized control of ammonia injection [16].

The above control strategy is mainly designed for a single working condition. In practical applications, as the load conditions change, the characteristic relationship between the amount of ammonia injected and the concentration of  $NO_x$  will change accordingly. It is difficult to adapt to the control task under the full load conditions using the controller under a single load condition. For this reason, Du Ming *et al.* proposed an improved fuzzy linear active disturbance rejection control strategy, which adjusts the parameters of the active disturbance rejection controller through error and fuzzy rules to improve the robustness of the control system [17]; Huang Xiaoying designed two-degree-of-freedom model-driven PID controllers under different load conditions, and improved the system's adaptability to variable conditions through the controller weighting scheme [18]; Zhang Jianhua *et al.* combined the internal model control fractional PID controller with the multi-model strategy to improve the system's control ability over the full range of load conditions [19].

In summary, many scholars use multi-parameter or multi-model strategies to improve the adaptability of the control system to the full range of work conditions. Among them, the multi-parameter strategy has a certain adaptability to the changes of small-scale working conditions, but is insufficient to adapt to the changes of large-scale working conditions. The multi-model strategy can adapt to changes in a wide range of working conditions, but in a certain working condition, because there is only one set of parameters, it cannot guarantee that it will always work at the optimal working point.

This paper combines the multi-parameter strategy with the multi-model strategy. An adaptive internal model control strategy for SCR denitration system based on multi-objective optimization is designed. This strategy is based on

two-degree-of-freedom internal model control (2-DOF-IMC). Taking advantage of its simple design, good control effect, and easy analysis [20], [21]. Compared with single-degree-of-freedom internal model control, it can achieve a separate design of system tracking performance and anti-disturbance performance. For a wide range of working condition changes, the control quality is mainly improved through the multi-model mechanism. For a small range of working condition changes, the control quality is further improved through a multi-parameter mechanism.

The adaptive characteristics of this strategy are manifested in two aspects:

- 1) Parameter adaptation. Aiming at the over-damping or under-damping that may occur when the actual work conditions deviate from the rated work conditions of the controller, a  $T - S$  fuzzy scheduler is used to design the controller parameter adaptive strategy. Through the weighted switching of different parameter sub-controllers, the adaptive ability of the control system to small-scale changes in working conditions is ensured.
- 2) Model adaptation. The model under typical work conditions is used to construct multiple two-degree-of-freedom internal model controllers. The recursive Bayesian probability weighting method is used to obtain the weight coefficients of each sub-model controller, which ensures the adaptive ability of the control system to a wide range of work conditions.

The design process and main contributions of the control system in this paper are:

- 1) Using the intelligent identification method based on DEQPSO, the transfer function of ammonia injection amount-outlet  $NO_x$  concentration under 3 typical work conditions is established. And use this model to establish a 2-DOF-IMC controller under various typical work conditions.
- 2) Using the NSGA-II multi-objective optimization algorithm based on chaotic mutation to solve the Pareto optimal solution of the parameters of the 2-DOF-IMC controller.
- 3) The  $T - S$  fuzzy scheduler is used to design the controller parameter adaptive strategy to solve the problem of under-damping or over-damping when the work conditions change in a small range.
- 4) The recursive Bayesian probability weighting method is used to design a multi-model adaptive strategy to improve the adaptability of the control system to changes in the full range of work conditions.
- 5) Taking a 600MW thermal power unit as the research object, the simulation verifies that the algorithm has good dynamic performance and anti-disturbance performance.

## II. INTRODUCTION OF SCR DENITRATION SYSTEM

The denitrification reaction requires a temperature of about  $960^\circ\text{C}$  without a catalyst. If a catalyst is used, the temperature

required for the reaction can be lowered between 300°C and 400°C. Therefore, the SCR denitration system is generally installed between the economizer and the air preheater. The temperature of this part of the flue gas provides a suitable temperature (300-400°C) for the SCR catalytic reaction [22]. A 600MW supercritical unit SCR denitration device is shown in Fig.1 [23].

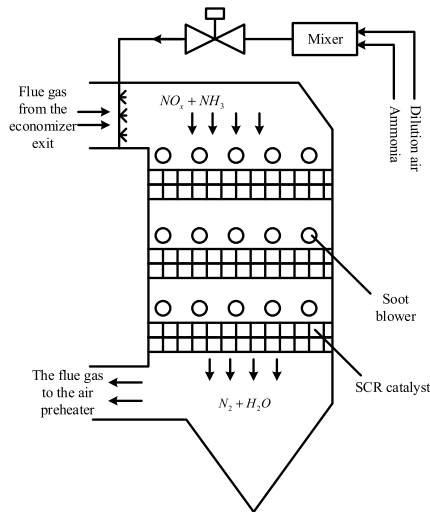
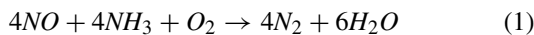


FIGURE 1. Schematic diagram of SCR denitration system.

The ammonia gas from the ammonia station is mixed with the dilution air from the air supply system. It is sprayed from the nozzle of the ammonia spraying grid. After being fully mixed with the flue gas at the outlet of the economizer, it flows through the catalyst. Under the action of the catalyst, it reacts with  $NO_x$ , reducing it to nitrogen and water, so as to achieve the purpose of denitration. The transformed product is free from pollution, the reaction runs stably, and the reliability is high. Under normal circumstances, the proportion of  $NO$  in the flue gas is about 95%, so the main chemical reaction equation of the denitration process is:



During the reaction, if the amount of ammonia injected is too small, it will prevent the  $NO_x$  and  $NH_3$  from fully reacting, resulting in the  $NO_x$  emission substandard [24]. If the ammonia injection is too large, it will cause the leakage of ammonia and cause secondary pollution. Moreover, excessive  $NH_3$  and  $SO_3$  react to synthesize hazardous by-products such as  $NH_4HSO_4$ . And it will block the orifice or cause catalyst failure, reduce the efficiency of denitration [25].

Therefore, the precise control of the amount of ammonia injection is the prerequisite for the high-quality work of the SCR system. The SCR system has the characteristics of large inertia and large delay, and it is not timely enough to adjust the speed using traditional PID and other control strategies. At the same time, when the unit load changes, the nonlinearity of the SCR system becomes prominent, and a single controller cannot meet the control requirements of nonlinearity and multiple operating conditions.

### III. IDENTIFICATION OF DYNAMIC CHARACTERISTICS OF SCR DENITRATION SYSTEM

#### A. DIFFERENTIAL EVOLUTION QUANTUM PARTICLE SWARM OPTIMIZATION

Quantum particle swarm optimization (QPSO) imparts quantum mechanical properties to particles in the solution space and enhances the full-space search capabilities of particles. It solves the problem of small randomness and difficult to globally converge in particle swarm optimization (PSO) algorithm [26]. In this paper, the differential evolution (DE) algorithm [27] is introduced into QPSO to form the differential evolution quantum particle swarm optimization (DEQPSO), which overcomes the shortcomings of being easy to fall into local optima in the later period of QPSO iteration.

Randomly generate  $m$  particles in the  $n$ -dimensional target search space, where the position of the  $i$ -th particle is  $X_i = (x_{i,1}, x_{i,2}, \dots, x_{i,n})$ ,  $i = 1, 2, \dots, m$ . The fitness of  $X_i$  can be calculated by substituting  $X_i$  into the objective function  $Q(X_i)$ . The smaller the objective function, the higher the fitness of  $X_i$ . Introducing the DE algorithm's population cooperation and competition mechanism. Randomly select particles for mutation, crossover, and selection operations to increase the diversity of the particle's entire life cycle. The mutation algorithm is:

$$V_{k1}(t) = X_{k1}(t) + f \cdot (X_{k2}(t) - X_{k3}(t)) \quad (2)$$

Among them,  $k1$ ,  $k2$ , and  $k3$  are random integers in the interval  $[1, m]$ ;  $X_{k1}(t)$  are randomly selected particles to be mutated;  $X_{k2}(t)$  and  $X_{k3}(t)$  are randomly selected auxiliary particles;  $f$  is a scaling parameter, usually taking a value of 0.5. Through the scaling of the auxiliary particle difference vector, the particle  $V_{k1}(t)$  after  $X_{k1}(t)$  mutation is obtained.

By replacing part of the attributes in  $X_{k1}(t)$  with the attributes of the corresponding positions in  $V_{k1}(t)$ , the particle  $U_{k1}(t)$  after  $X_{k1}(t)$  crosses is obtained. The crossover algorithm is:

$$u_{k1,j}(t) = \begin{cases} v_{k1,j}(t) & c < cr \text{ or } j = rnd \\ x_{k1,j}(t) & \text{else} \end{cases} \quad (3)$$

In the equation,  $v_{k1,j}(t)$  is the  $j$ -th attribute of  $V_{k1}(t)$ ;  $u_{k1,j}(t)$  is the  $j$ -th attribute of  $U_{k1}(t)$ ;  $cr$  is the crossover coefficient, which is generally 0.75~1;  $c$  is a random number in interval  $[0, 1]$ ;  $rnd$  is a random integer in interval  $[1, m]$ , Ensure that  $U_{k1}(t)$  is inherited from  $V_{k1}(t)$  by at least one dimension attribute.

The greedy way is used for one-to-one survival competition, and the selection equation is:

$$X_{k1}(t) = \begin{cases} U_{k1}(t) & Q(U_{k1}(t)) < Q(X_{k1}(t)) \\ X_{k1}(t) & \text{else} \end{cases} \quad (4)$$

The optimal position experienced by particle  $i$  is denoted as  $X\_best_i = (x\_best_{i,1}, x\_best_{i,2}, \dots, x\_best_{i,n})$ , and the fitness is denoted as  $Q\_best_i$ . The optimal position experienced by all particles is denoted as  $X\_best_g = (x\_best_{g,1}, x\_best_{g,2}, \dots, x\_best_{g,n})$ , and the fitness is

denoted as  $Q\_best_g$ . Define the average value  $X\_best_a$  of the optimal position of all individual particles as:

$$X\_best_a = (x\_best_{a,1}, \dots, x\_best_{a,n}) \\ = \left( \frac{1}{m} \sum_{i=1}^m x\_best_{i,1}, \frac{1}{m} \sum_{i=1}^m x\_best_{i,n} \right) \quad (5)$$

The particle position is updated by combining the information of the individual particle's optimal position  $X\_best_i$ , the overall particle's optimal position  $X\_best_g$ , and the average value of the overall particle's optimal position  $X\_best_a$ . As shown in (6)~(8):

$$p_{i,j}(t) = r \cdot x\_best_{i,j}(t) + (1 - r) \cdot x\_best_{g,j}(t) \quad (6)$$

$$x_{i,j}(t + 1) = p_{i,j}(t) \pm \beta(t) |x\_best_{a,j}(t) - x_{i,j}(t)| \ln \left( \frac{1}{u} \right) \quad (7)$$

$$\beta(t) = 1 - \frac{t}{T} \cdot 0.5 \quad (8)$$

In the equation,  $j = 1, 2, \dots, n$ ;  $r$  and  $u$  are random numbers on the interval  $[0, 1]$ ;  $t$  is the current iteration algebra;  $T$  is the maximum iteration algebra;  $\beta$  is the scaling factor, which linearly decreases from 1 to 0.5 according to the iteration algebra. The flow chart of DEQPSO algorithm is shown in Fig.2.

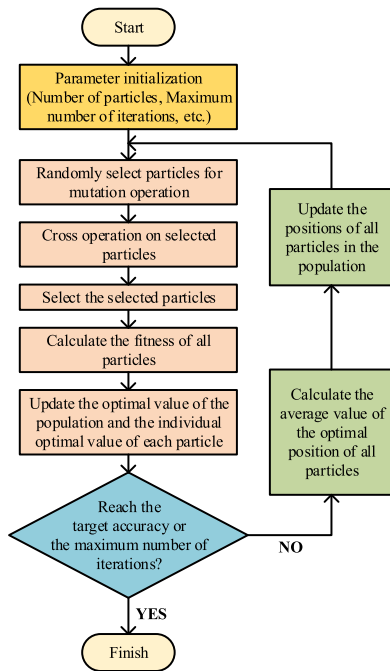


FIGURE 2. Flow chart of DEQPSO algorithm.

In order to prove the effectiveness of the DEQPSO algorithm, five standard test functions are selected to test the PSO, QPSO, and DEQPSO algorithms. Among them,  $f_4$  and  $f_5$  have multiple optimal value points, which can test the global search ability of the algorithm. The test function information is shown in Table 1.

TABLE 1. Information about the test function.

Test function	Search range	Theoretical optimal solution
$f_1(x) = \sum_{i=1}^n x_i^2$	$[-100,100]^n$	0
$f_2(x) = \max\{ x_i , 1 \leq i \leq n\}$	$[-100,100]^n$	0
$f_3(x) = \sum_{i=1}^n \left( \sum_{j=1}^i x_j^2 \right)^2$	$[-100,100]^n$	0
$f_4(x) = \frac{1}{4000} \sum_{i=1}^n x_i^2 - \prod_{i=1}^n \cos\left(\frac{x_i}{\sqrt{i}}\right) + 1$	$[-100,100]^n$	0
$f_5(x) = \sum_{i=1}^n ( x_i + 0.5 )^2$	$[-5,5]^n$	0

Set the search dimension to 30 and the maximum number of iterations to 500. Each algorithm was independently run 30 times for each test function. The algorithm test results are shown in Table 2. It can be seen from the table that, whether it is the mean or the median, DEQPSO has the highest accuracy, QPSO is the second, and PSO is the lowest. It shows that the algorithm in this paper has stronger global search ability and more general applicability than before.

The Friedman test and the Friedman rank test [28], [29] were used to compare the quality of the analytical solutions. The results are shown in Table 3. It can be seen from the table that the correlation between the solutions of the DEQPSO algorithm is the highest, followed by the QPSO, and the PSO is the lowest.

In terms of the time complexity of the algorithm, for PSO and QPSO, the time complexity is  $O(m \times n)$ . The DEQPSO algorithm adds mutation, crossover, and selection operations, and the time complexity of the added operations is  $O(m \times n)$ . So the time complexity of the overall algorithm is still  $O(m \times n)$ . Therefore, in terms of time complexity, this algorithm remains unchanged compared to the original algorithm.

Calculate the time-consuming of the algorithm by simulating the test function. For the test functions in Table 1, the same number of iterations and populations were used to run 30 times independently, and the results shown in Table 4 were obtained. It can be seen from the table that DEQPSO takes the longest time, QPSO is the second, and PSO is the shortest, but the difference in time duration is not large, and the increased computation and excessive consumption are limited.

**B. INTELLIGENT IDENTIFICATION METHOD BASED ON DEQPSO**

The objective function uses the mean square error function (MSE) [28]:

$$Q(X_i) = \frac{1}{l} \sum_{k=1}^l [y(kT_s) - \tilde{y}(kT_s)]^2 \\ = \frac{1}{l} \sum_{k=1}^l \{y(kT_s) - f_g[u(kT_s), X_i]\}^2 \quad (9)$$

**TABLE 2. The test results of the accuracy of the three algorithms.**

Test function	PSO		QPSO		DEQPSO	
	Mean	Median	Mean	Median	Mean	Median
$f_1$	$1.80 \times 10^{-3}$	$1.20 \times 10^{-3}$	$5.59 \times 10^{-9}$	$8.18 \times 10^{-9}$	$1.89 \times 10^{-19}$	$2.06 \times 10^{-19}$
$f_2$	8.1	7.4	$7.59 \times 10^{-7}$	$4.90 \times 10^{-8}$	$1.08 \times 10^{-10}$	$1.91 \times 10^{-10}$
$f_3$	$4.10 \times 10^{-3}$	$2.20 \times 10^{-3}$	$5.23 \times 10^{-15}$	$1.01 \times 10^{-14}$	$1.36 \times 10^{-15}$	$2.11 \times 10^{-15}$
$f_4$	0.01	0.0081	0.0104	0.0221	0.0071	0.0069
$f_5$	1.6395	1.5201	$2.87 \times 10^{-33}$	$1.54 \times 10^{-33}$	$3.15 \times 10^{-40}$	$2.96 \times 10^{-40}$

**TABLE 3. Results of friedman’s test and friedman’s aligned ranks test.**

Algorithm	Friedman		Friedman Aligned		
	Score	Rank	Algorithm	Score	Rank
PSO	3.7258	3	PSO	37.2528	3
QPSO	3.1627	2	QPSO	36.2544	2
DEQPSO	2.8916	1	DEQPSO	34.1485	1

In the equation,  $T_s$  is the sampling time;  $u(kT_s)$  is the collected input sequence;  $y(kT_s)$  is the collected output sequence;  $f_g$  is the estimated model to be identified;  $\tilde{y}(kT_s)$  is the output of the estimated model;  $X_i$  records the parameters of the estimated model. For the process system, the commonly used model structure of estimated model  $f_g$  is [29]:

$$Y(s) = \frac{K(\alpha + \beta s)e^{-\tau s}}{s^n(Ts + 1)^n} \quad (10)$$

In the equation,  $K$  is the system gain;  $\tau$  is the pure delay time;  $T$  is the system inertia time;  $n$  is the order of the inertial part;  $\beta$  is the differential time constant. The dynamic model of the SCR denitration system can be fitted with a high-order inertial model with pure delay. The model structure is:

$$Y(s) = \frac{Ke^{-\tau s}}{(Ts + 1)^n} \quad (11)$$

The difference equation of the model is:

$$\begin{aligned} x_1(k+1) &= e^{-DT/T}x_1(k) + K(1 - e^{-DT/T})u(k) \\ x_{2 \sim n}(k+1) &= e^{-DT/T}x_{2 \sim n}(k) \\ &\quad + (1 - e^{-DT/T})x_{1 \sim n-1}(k+1) \\ y(k+1) &= x_n(k+1 - \tau/DT) \end{aligned} \quad (12)$$

The DEQPSO optimization algorithm is used to identify the parameters in the estimated model (11). Finally find the parameter that minimizes the objective function  $Q$ .

**C. IDENTIFICATION RESULTS OF DYNAMIC CHARACTERISTICS**

Taking a 600MW thermal power unit as the research object, the ammonia injection disturbance test was carried out under three load conditions (350MW, 450MW and 550MW). The ammonia injection and the SCR outlet  $NO_x$  concentration data were collected. The sampling time was 5s. Eliminate outliers in the collected data. In order to eliminate the influence of measurement noise, inertial filtering is used for data smoothing.

**TABLE 4. The test results of the time-consuming cases of the three algorithms.**

Test funcio n	PSO		QPSO		DEQPSO	
	Mean /s	Optimal /s	Mean /s	Optimal /s	Mean /s	Optimal /s
$f_1$	19.45	16.18	20.52	18.83	21.48	20.36
$f_2$	17.66	15.76	18.14	17.30	18.71	18.04
$f_3$	19.89	18.15	21.45	20.08	22.81	21.50
$f_4$	21.51	21.16	24.35	24.07	27.22	26.61
$f_5$	21.82	18.37	22.76	20.59	22.91	21.46

Before identifying the dynamic characteristics of the system, the steady-state component in the data should be eliminated. In traditional methods, multi-point averaging is often used to obtain steady-state components, which has low accuracy and affects the identification accuracy. In this paper, the input and output steady-state components of the system are used as the parameters to be identified. The improved system estimation model structure (11) is transformed into

$$Y(s) - y_0 = \frac{Ke^{-\tau s}}{(Ts + 1)^n} (U(s) - u_0) \quad (13)$$

In the equation,  $u_0$  and  $y_0$  are the steady-state components of the input and output of the system.

In order to avoid subjective will and accidental factors, the first half of the data is used for model training, and the second half of the data is used for model testing. The identification results are shown in Table 5. Fig.3, Fig.4, and Fig.5 show the comparison of model output and actual data under three load conditions.

It can be seen that the model output fits the actual data well, which can meet the model requirements of the 2-DOF-IMC. The model test results show that the model has a high degree of accuracy and no over-fitting phenomenon has occurred.

**IV. DESIGN OF TWO-DEGREE-OF-FREEDOM INTERNAL MODEL CONTROL SYSTEM**

**A. TWO-DEGREE-OF-FREEDOM INTERNAL MODEL CONTROL**

Horowitz first proposed the idea of two degrees of freedom in the 1960s [30]. The structure of the 2-DOF-IMC system is shown in Fig.6 [31].

In the Fig.6,  $Q_1(s)$  and  $Q_2(s)$  constitute a 2-DOF-IMC controller;  $G_p(s)$  is the controlled object;  $G_m(s)$  is the estimated



the form of additive uncertainty, namely

$$G_p(s) = G_m(s) + \Delta(s) \quad (19)$$

In the equation,  $\Delta(s)$  represents the additive perturbation of model uncertainty. The system internal disturbance  $R_1(s)$  and external disturbance  $R_2(s)$  can be equivalent to a part of the model uncertainty and are no longer considered separately. Fig.6 can be transformed into the structure shown in Fig.7 by (19).

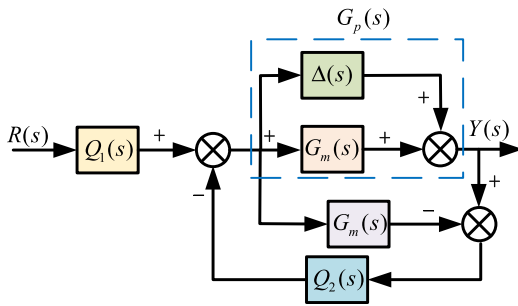


FIGURE 7. 2-DOF-IMC equivalent block diagram 1.

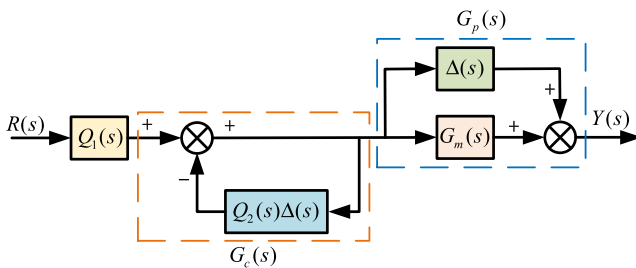


FIGURE 8. 2-DOF-IMC equivalent block diagram 2.

The equivalent transformation of Fig.7 can obtain the open-loop control system structure shown in Fig.8.

It can be seen from Fig.8 that as long as the controllers  $Q_1(s)$ ,  $G_c(s)$  and the controlled system  $G_p(s)$  are stable, the system is stable. According to the principle of small gain, the necessary and sufficient condition for  $G_c(s)$  to be stable is

$$\|Q_2(j\omega)\Delta(j\omega)\|_\infty = \left\| \frac{G_m^{-1}(j\omega)}{(\lambda_2 j\omega + 1)^n} \Delta(j\omega) \right\|_\infty < 1 \quad (20)$$

From the stability of  $G_p(s)$ , we know that the model uncertainty  $\Delta(s)$  must have an upper bound. Therefore, by adjusting  $\lambda_2$ ,  $G_c(s)$  can always meet the stability condition (20).

### C. NSGA-II BASED ON CHAOTIC MUTATION

Srinivas and Deb proposed NSGA-II on the basis of NSGA in 2000. The new algorithm introduces the elite strategy, and proposes a fast non-dominated sorting algorithm and a crowding degree comparison operator. It has the advantages of fast calculation speed and good convergence [32]. In order to solve the shortcoming of NSGA-II that is easy to fall into local optimum, this paper proposes a NSGA-II based on chaotic mutation.

The chaotic iteration strategy is used to initialize the population to reduce the influence of random distribution on

the optimization results [33]. Tent chaotic mapping has the advantage of uniform distribution [34], and its mapping equation is

$$x_{n+1} = \begin{cases} \mu \cdot (1 - x_n) \\ \mu \cdot x_n \end{cases} \quad (21)$$

Randomly generate vector  $X_0 = (x_{0,1}, x_{0,2}, \dots, x_{0,n})$ , where  $n$  is the number of parameters to be optimized. Bring each component in  $X_0$  into (21) and iterate  $m$  times to generate initial individuals  $X_1 \sim X_m$ . Use (22) to map the population to the solution space:

$$x_{i,j} = \min_j + x_{i,j} \cdot (\max_j - \min_j) \quad (22)$$

In the equation,  $\min_j$  and  $\max_j$  are the upper and lower limits of the  $j$ -th parameter to be optimized.

Calculate the fitness function  $Q_i = (q_{i,1}, q_{i,2}, \dots, q_{i,d})$  of each individual, where  $d$  is the number of optimization goals. In order to avoid the group being brought into the local optimal solution by the prominent individuals in the initial stage of the search, (23) is used to improve the fitness function and enlarge the fitness gap between individuals.

$$q_{i,k} = q_{i,k} \cdot e^{(1+\lambda|q_{i,k}|)} \quad (23)$$

In the equation,  $\lambda$  is the adjustment factor.

Perform non-dominated sort according to the fitness function to obtain front  $F_1, F_2, \dots$ . Use (24) to calculate the crowding distance  $I_l$  of the  $l$ -th individual in the front:

$$I_l = \begin{cases} \infty & l = 1 \text{ or } g \\ \sum_{j=1}^n \frac{q_{l-1,j} - q_{l+1,j}}{\max_j - \min_j} & 1 < l < g \end{cases} \quad (24)$$

The selection operation is based on the binary tournament strategy [35]. Equation (25) and (26) are used for crossover and mutation to generate individual offspring.

$$\begin{cases} x_{i1,j}(t+1) = \frac{1}{2} [(1 - \beta_j) x_{i1,j} + (1 + \beta_j) x_{i2,j}] \\ x_{i2,j}(t+1) = \frac{1}{2} [(1 + \beta_j) x_{i1,j} + (1 - \beta_j) x_{i2,j}] \end{cases} \quad (25)$$

$$x_{i3,j}(t+1) = x_{i3,j}(t) + (\max_j - \min_j) \delta_j \quad (26)$$

In the equation,  $i1, i2, i3$  are random integers in the interval  $[1, m]$ ;  $\beta_k$  is the cross factor;  $\delta_k$  is the variation factor.

Perform non-dominated sort on all individuals of the parent and offspring, and calculate the crowding distance in each front. Individuals are selected according to the principle that the lower the front rank, the more priority, and the larger the crowding distance of the same front rank, the more priority.

Traverse the individuals in each front. If the crowding distance between two individuals is less than the threshold  $\sigma$ , then the two individuals are considered to be similar in quality, one individual is randomly retained, and chaotic mutation is added to the other individual [36] to increase the diversity of individuals while avoiding falling into the local optimum:

$$X_i = (1 - \alpha \cdot \varepsilon) \cdot X_i + (-1)^i \cdot \alpha \cdot \varepsilon \cdot X_i / \|X_i\| \quad (27)$$

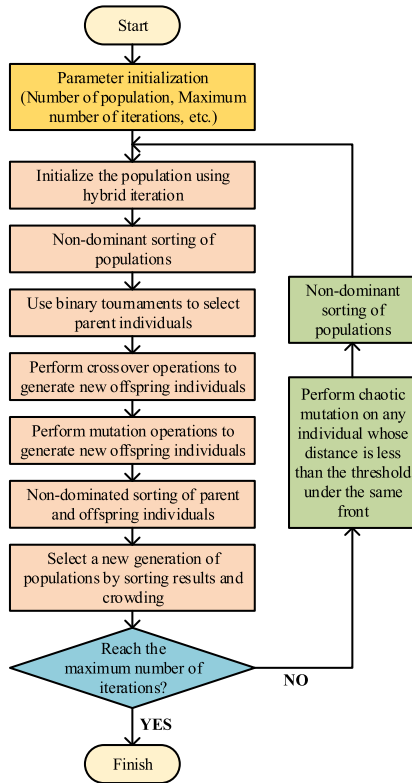


FIGURE 9. Flow chart of NSGA-II algorithm based on chaotic mutation.

In the equation,  $\alpha$  is the influencing factor of artificial degradation;  $\varepsilon$  is the chaotic disturbance factor.

The flow chart of NSGA-II algorithm based on chaotic mutation is shown in Fig.9.

**D. CONTROL SYSTEM DESIGN AND PARAMETER TUNING**

The corresponding 2-DOF-IMC controller is designed using the dynamic models under the load of 350MW, 450MW and 550MW established in 2.3. The pure delay  $e^{-\tau s}$  is realized by the first-order Taylor approximation. The order of  $Q_1(s)$  and  $Q_2(s)$  is selected as the second order. Table 6 shows the design results of the 2-DOF-IMC controller under various typical load conditions.

Use 350~550MW as the research interval to adjust the parameter optimization range according to the robust stability condition (20). The system is required to be closed-loop stable when the 2-DOF-IMC under typical work conditions is used to control the 350~550MW full-working model.

The maximum uncertainty additive perturbation  $\Delta_{max}(j\omega)$  of typical work condition model and full work condition model is  $\pm (G_{p550}(j\omega) - G_{p350}(j\omega))$ . Because the analytic solution of  $\lambda_2$  under condition  $\|Q_2(j\omega)\Delta(j\omega)\|_\infty < 1$  is difficult to find. Therefore, the selection of  $\lambda_2$  is qualitatively analyzed and calculated by means of simulation and drawing of Bode diagram. The log-amplitude-frequency characteristic curves of  $Q_2(j\omega)\Delta_{max}(j\omega)$  under different parameters  $\lambda_2$  were drawn when the 2-DOF-IMC controller was adopted under various typical working conditions. The curve is shown in Fig.10.

TABLE 6. 2-DOF-IMC controller under various typical working conditions.

Load(MW)	$Q_1(s)$	$Q_2(s)$
350	$\frac{(184s+1)^2}{-0.2705(\lambda_1s+1)^2}$	$\frac{(184s+1)^2}{-0.2705(\lambda_2s+1)^2}$
450	$\frac{(154s+1)^2}{-0.2429(\lambda_1s+1)^2}$	$\frac{(154s+1)^2}{-0.2429(\lambda_2s+1)^2}$
550	$\frac{(134s+1)^2}{-0.1954(\lambda_1s+1)^2}$	$\frac{(134s+1)^2}{-0.1954(\lambda_2s+1)^2}$

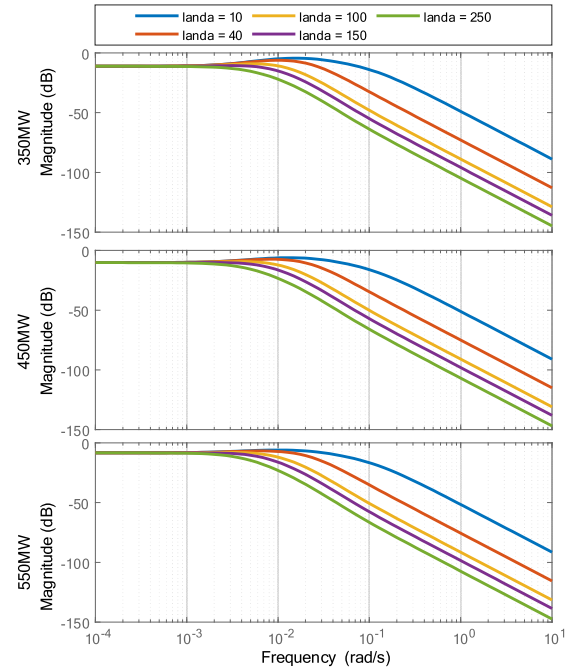


FIGURE 10. Logarithmic amplitude-frequency characteristic curve of  $Q_2(j\omega)\Delta_{max}(j\omega)$  under internal model of each typical working condition.

As can be seen from the figure, at the same frequency  $\omega$ , with the decrease of  $\lambda_2$ ,  $|Q_2(j\omega)\Delta_{max}(j\omega)|$  gradually approaches and may exceed 1, and the robust stability of the system becomes worse. With the increase of  $\lambda_2$ ,  $|Q_2(j\omega)\Delta_{max}(j\omega)|$  gradually decreases, and the robust stability of the system is enhanced.

Therefore, after comprehensive consideration, the tuning interval of  $\lambda_2$  is selected as [40, 150]. To ensure that the closed-loop system is stable while maintaining a certain response speed. Parameter  $\lambda_1$  only needs to satisfy  $\lambda_1 > 0$ . In this system, in order to avoid the drastic action of the controller, the tuning interval of  $\lambda_1$  is set as [40, 150].

The parameters  $\lambda_1$  and  $\lambda_2$  are tuned using the NSGA-II multi-objective optimization algorithm based on chaotic mutation. The fitness function is selected as follows:

$$\begin{aligned}
 q_1 &= \frac{1}{l} \sum_{k=1}^l [r(kT_s) - y(kT_s)]^2 \quad r(t) \neq 0, \quad r_1(t) = 0 \\
 &= \frac{1}{l} \sum_{k=1}^l [r(kT_s) - f_g[u_1(kT_s)]]^2 \quad r_2(t) = 0 \quad (28)
 \end{aligned}$$



$$q_2 = \frac{1}{l} \sum_{k=1}^l [y(kT_s)]^2 \quad r(t) = 0, \quad r_1(t) \neq 0$$

$$= \frac{1}{l} \sum_{k=1}^l [f_g [u_2(kT_s)]]^2 \quad r_2(t) \neq 0 \quad (29)$$

$$q_3 = \frac{1}{l} \sum_{k=1}^l [u_1(kT_s)]^2 + \frac{1}{l} \sum_{k=1}^l [u_2(kT_s)]^2 \quad (30)$$

In the equation,  $l$  is the sampling length;  $y = f(u)$  is the controlled system;  $u_1$  is the control quantity of the system under the set point step response;  $u_2$  is the control quantity of the system when overcoming internal and external disturbances;  $q_1$  reflects the performance of the system following the set point  $r(t)$ ;  $q_2$  reflects the performance of the system to eliminate internal and external disturbances  $r_1(t)$  and  $r_2(t)$ ;  $q_3$  reflects the system's consumption of control energy. In order to avoid the control effect being too violent or gentle, the optimal interval between  $\lambda_1$  and  $\lambda_2$  is set as [40, 150]. The solved Pareto optimal solution is shown in Fig.11~Fig.13.

The Pareto optimal solution is divided into five areas (AreaI~AreaV). The solutions in AreaI have the strongest set point tracking performance and consumes the most control energy. From AreaI to AreaV, the set point tracking performance of the control system gradually decreases, and the control energy consumed also gradually decreases.

**E. SIMULATION TEST AND ANALYSIS**

In AreaI~AreaV, five controller parameters (ParametersI~ParametersV) are selected according to the principle of strongest anti-disturbance ability and centered distribution. The parameters are shown in Table 7.

The 2-DOF-IMC controller shown in Table 6 and the control parameters shown in Table 7 are used to control the SCR denitration system under various typical load conditions. In 200s, a set point step signal with an amplitude of 1 is added,

an internal disturbance signal with an amplitude of  $-0.4$  is added at 2000s, and an external disturbance signal with an amplitude of  $-0.1$  is added at 4000s. The simulation results are shown in Fig.14~Fig.16. The quantitative performance indexes are shown in Table 8, where  $M_p$  is the overshoot of step response,  $T_s$  is the system stability time ( $\pm 0.02$ ),  $MSE_1$  is the mean square error of the system response from 0 to 2000s (reflecting the dynamic performance of the system),  $MSE_2$  is the mean square error of the system response from 2001 to 6000s (reflecting the anti-disturbance performance of the system), and  $E$  is the mean square control quantity of the system.

It can be seen from Fig.14~Fig.16 and Table 8 that although the system responds most quickly under ParametersI, it also consumes huge control energy and causes the violent action of the controller. Although the controller moves smoothly under ParametersV, the system response is under damped and the rapidity is poor. Parameter  $\lambda_1$  determines the set point tracking performance of the system. As  $\lambda_1$  increases, the overshoot of the system response will gradually decrease, the rapidity of the system will decrease, the consumption of the control quantity will be weakened, and the stability of the control will increase. The parameter  $\lambda_2$  determines the anti-disturbance performance of the system. The smaller the  $\lambda_2$ , the stronger the system's ability to eliminate disturbances. The set point tracking performance and anti-disturbance ability of the system can be adjusted by adjusting  $\lambda_1$  and  $\lambda_2$ , which is the advantage of the two-degree-of-freedom controller.

At the same time, the 2-DOF-IMC is better than PID in terms of adjustment speed, overshoot, and anti-disturbance ability. This is mainly because the model information of the controlled object is added to the internal model controller, which is an "active" adjustment method compared to PID.

Increase or decrease the proportional coefficient, inertia time, and pure delay of the controlled object by 5% to test

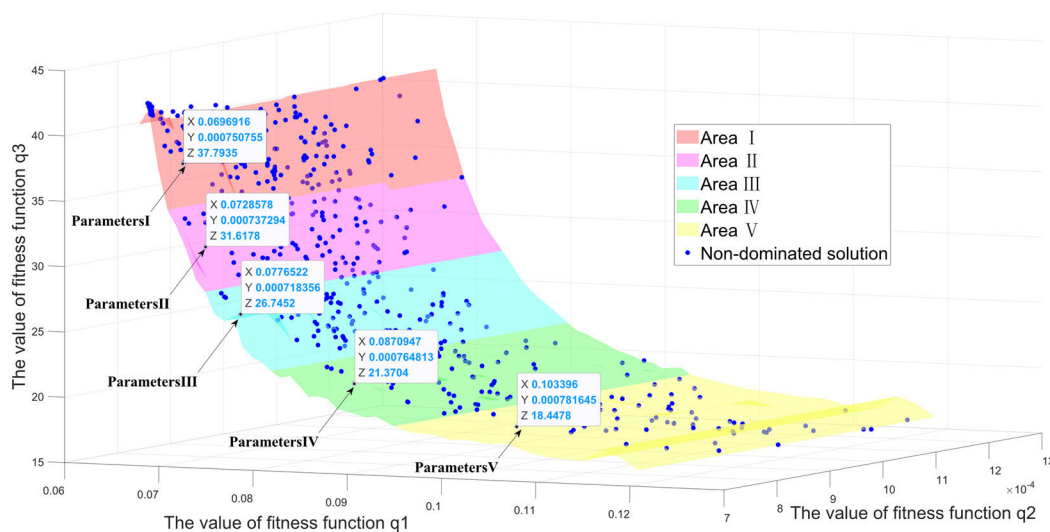


**FIGURE 11. Pareto optimal solution of controller parameters under 350MW load condition.**

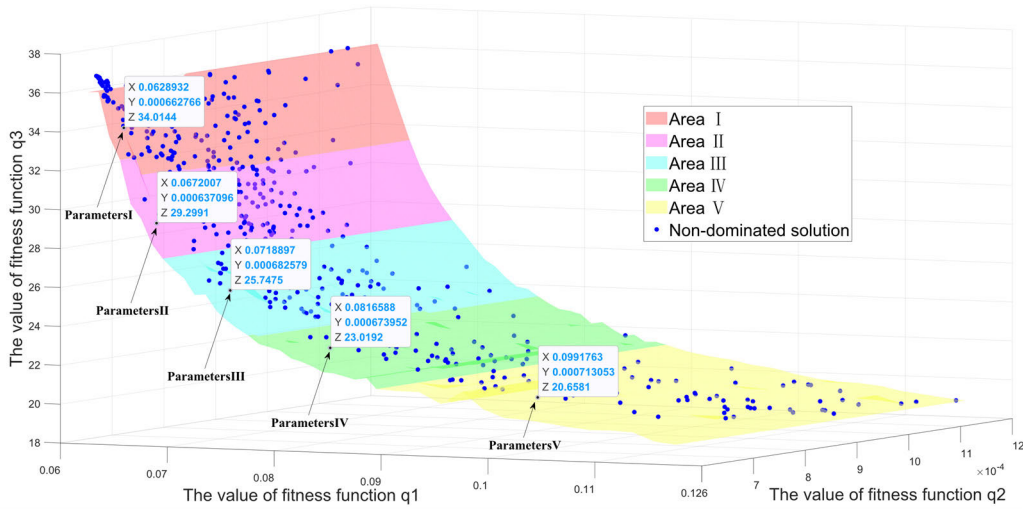


FIGURE 12. Pareto optimal solution of controller parameters under 450MW load condition.

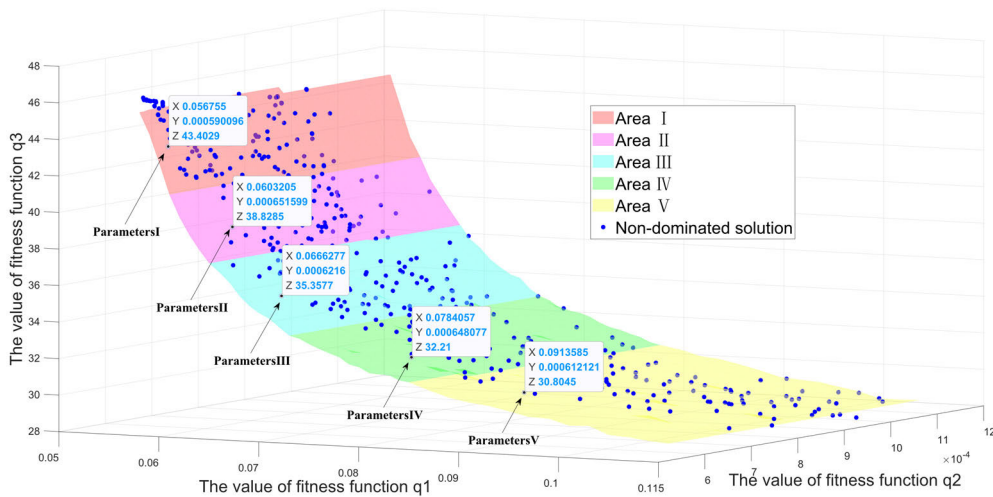


FIGURE 13. Pareto optimal solution of controller parameters under 550MW load condition.

TABLE 7. Parameter tuning results of 2-DOF-IMC controller under various typical working conditions.

Load (MW)	Name	Parameters				
		I	II	III	IV	V
350	$\lambda_1$	42.82	49.10	58.71	78.44	111.74
	$\lambda_2$	49.50	46.77	42.90	52.33	55.70
450	$\lambda_1$	42.59	51.16	61.09	80.99	116.72
	$\lambda_2$	46.05	40.82	50.05	48.31	56.16
550	$\lambda_1$	42.92	50.46	63.21	87.25	113.36
	$\lambda_2$	45.11	57.54	51.50	56.83	49.50

the robustness of the 2-DOF-IMC. The results are shown in Fig.17~Fig.19. The quantitative performance indexes are shown in Table 9, where  $M_p$  is the overshoot of step response,  $T_s$  is the system stability time ( $\pm 0.02$ ),  $MSE$  is the mean square error of the system response, and  $E$  is the mean square control quantity of the system.

It can be seen from the figure that the 2-DOF-IMC has strong robustness under each parameter and can effectively overcome the model mismatch. With the increase of load, the system control quality develops to underdamping direction, and with the decrease of load, the system control quality develops to overdamping direction.

## V. DESIGN OF AN ADAPTIVE TWO-DEGREE-OF-FREEDOM INTERNAL MODEL CONTROL SYSTEM

### A. CONTROLLER PARAMETER ADAPTIVE STRATEGY

From the transfer function of the system under typical load conditions shown in Table 5, it can be seen that as the load increases, the dynamic characteristics of the SCR denitration system become more active (Inertial time becomes smaller), and the system response speed increases. Combined with the analysis of Fig.17(b), Fig.18(b) and Fig.19(b), it can be obtained that the control quality of the system develops in the direction of underdamping. In this case, the parameters

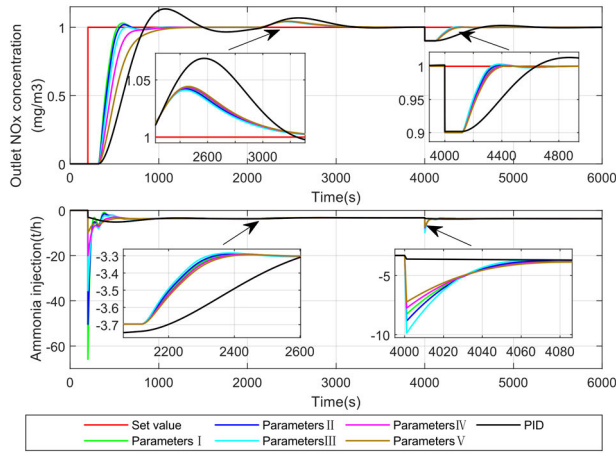


FIGURE 14. Simulation results of 2-DOF-IMC under 350MW load condition.

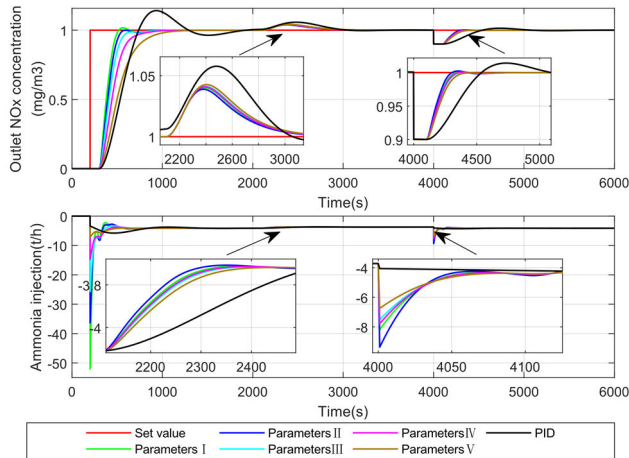


FIGURE 15. Simulation results of 2-DOF-IMC under 450MW load condition.

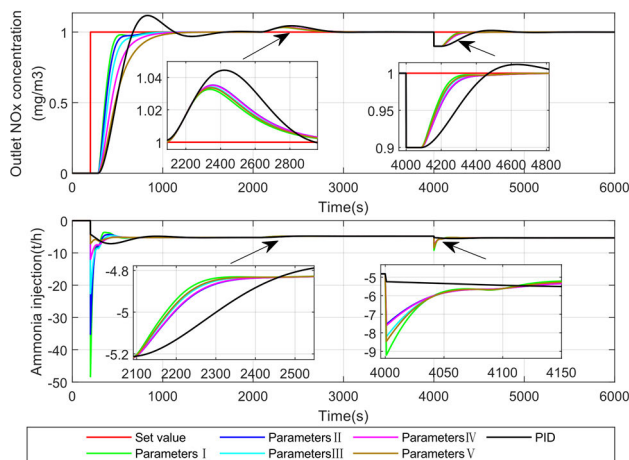


FIGURE 16. Simulation results of 2-DOF-IMC under 550MW load condition.

with strong control effect should be adopted to improve the response speed of the system (such as ParametersI, ParametersII).

TABLE 8. Comparison of dynamic performance indexes of 2-dof-imc under various typical load conditions.

Load (MW)	Parameters	Dynamic performance indicators				
		$M_p$ /%	$T_s$ /s	$MSE_1$ / $10^{-2}$	$MSE_2$ / $10^{-4}$	$E$
350	I	3.04	640	8.71	6.27	21.31
	II	1.94	542	9.11	6.12	18.66
	III	0	584	9.71	5.91	16.47
	IV	0	790	10.89	6.43	14.54
	V	0	1000	12.92	6.62	13.39
	PID	13.48	1997	16.31	13	13.15
450	I	1.74	500	7.89	5.34	21.51
	II	0	537	8.40	5.08	19.40
	III	0	609	8.9	5.55	18.15
	IV	0	806	10.21	5.46	16.98
	V	0	997	12.4	5.87	16.11
	PID	14.14	1720	13.82	10.01	16.36
550	I	0.28	491	7.09	4.42	30.25
	II	0	541	7.54	4.98	28.53
	III	0	647	8.33	4.71	27.01
	IV	0	807	9.8	4.95	25.76
	V	0	957	11.42	4.62	25.08

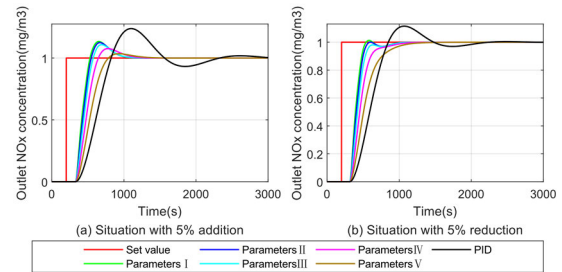


FIGURE 17. Robustness test results of 2-DOF-IMC under 350MW load condition.

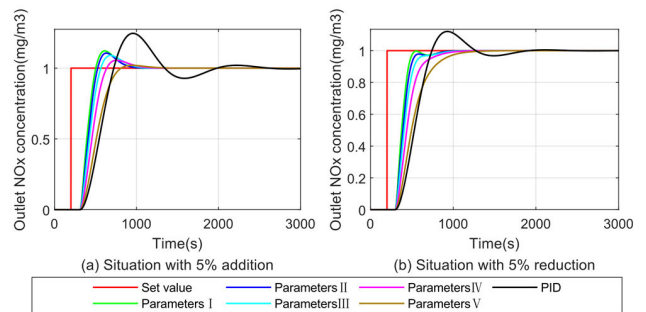


FIGURE 18. Robustness test results of 2-DOF-IMC under 450MW load condition.

As the load decreases, the dynamic characteristics of the SCR denitration system slow down (Inertia time becomes larger). The system response speed becomes slow. Combined with the analysis of Fig.17(a), Fig.18(a) and Fig.19(a), it can be obtained that the system control quality develops in the direction of over-damping. At this time, control parameters with weak control effect should be used to avoid excessive overshoot (such as ParametersIV, ParametersV).

Considering that the controller action is too violent under ParametersI and the controller action is too slow under ParametersV, so the control parameters in AreaI and AreaV

**TABLE 9. Comparison of dynamic performance indexes of robustness test of 2-dof-imc under various typical load conditions.**

Load (MW)	Parameters	Dynamic performance indicators							
		Situation with 5% addition				Situation with 5% reduction			
		$M_p / \%$	$T_s / s$	$MSE / 10^{-2}$	$E$	$M_p / \%$	$T_s / s$	$MSE / 10^{-2}$	$E$
350	I	13.40	947	6.43	28.62	0	908	5.57	31.60
	II	12.51	949	6.68	23.33	0	915	5.84	26.25
	III	10.79	954	7.05	18.98	0	927	6.25	21.81
	IV	7.65	1056	7.78	15.20	0	1010	7.06	17.99
	V	3.49	1114	9.02	12.93	0	1144	8.47	15.68
	PID	23.83	2200	11.88	12.64	8.4296	1865	10.52	15.17
450	I	12.19	873	5.75	25.28	0	783	5.16	28.14
	II	10.64	869	6.09	21.07	0	791	5.52	23.87
	III	8.96	941	6.46	18.63	0	813	5.92	21.40
	IV	5.6	974	7.20	16.32	0	875	6.74	19.05
	V	1.98	771	8.54	14.63	0	1046	8.23	17.38
	PID	24.60	1883	10.08	15.29	12.09	1679	9.08	17.85
550	I	10.90	823	5.17	31.93	0	710	4.65	36.41
	II	9.70	897	5.46	28.56	0	721	4.95	32.99
	III	7.50	902	5.94	25.56	0	762	5.49	29.93
	IV	4.34	963	6.85	23.13	0	868	6.48	27.44
	V	0.95	756	7.82	21.78	0	996	7.58	26.05
	PID	24.37	1660	8.70	23.18	11.74	1476	7.83	27.28

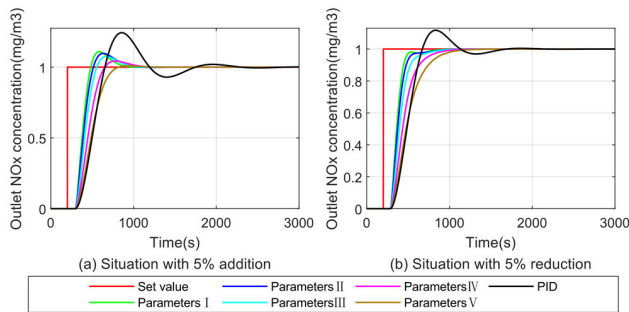


**FIGURE 19. Robustness test results of 2-DOF-IMC under 550MW load condition.**

are discarded. ParametersII, ParametersIII, ParametersIV are used to design the controller parameter adaptive strategy.

The design idea is to use ParametersII, ParametersIII, ParametersIV to design sub-controllersI, sub-controllersII and sub-controllersIII. The total control quantity is obtained by the weighted summation of the outputs of the three sub-controllers. When the load is at the model rated load, the output of sub-controllerII accounts for the largest proportion. When the load positively deviates from the model rated load, the output weight of sub-controllerI gradually increases. When the load deviates from the model rated load in the reverse direction, the output weight of sub-controllerIII gradually increases.

The output weighting of the sub-controller is completed by the scheduler based on the  $T - S$  fuzzy model [37]. Suppose that the  $T - S$  fuzzy model is composed of  $n$  fuzzy rules, and the  $i$ -th rule is [38]:

$$R^i : \text{if } x_1 \text{ is } A_1^i \text{ and } x_2 \text{ is } A_2^i, \dots, x_n \text{ is } A_n^i$$

$$\text{Then } y^i = p_0^i + p_1^i x_1 + p_2^i x_2 + \dots + p_n^i x_n \quad (31)$$

In the equation,  $R^i$  is the  $i$ -th fuzzy rule;  $x_j$  is the  $j$ -th input variable;  $n$  is the number of input variables;  $y^i$  is the output

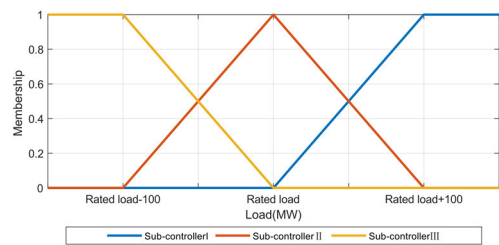


**FIGURE 20. The membership curve of each sub-controller under the controller parameter adaptive strategy.**

of the  $i$ -th rule;  $p_j^i$  is the  $j$ -th parameter of the  $i$ -th rule;  $A_j^i$  is the value when the membership of the  $j$ -th input variable is 1 under the  $i$ -th fuzzy rule.

After the output  $y^i$  of each rule is weighted and averaged according to a certain weight, the output  $y$  of the scheduler can be obtained:

$$y = \frac{\sum_{i=1}^n w^i y^i}{\sum_{i=1}^n w^i} \quad (32)$$

The weighting coefficient is the product of the membership degrees of the input variables:

$$w^i = \prod_{j=1}^n \mu_{A_j^i}(x_j) \quad (33)$$

The membership function adopts the trigonometric function, and the membership curve of each sub-controller is shown in Fig.20.

Fig.6 can be equivalent transformed into a set point filtered 2-DOF control structure as shown in Fig.21.

In the Fig.21, the set point filter  $C_1(s)$  is

$$C_1(s) = \frac{Q_1(s)}{Q_2(s)} \quad (34)$$

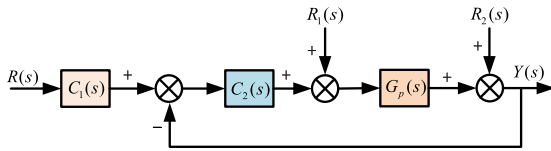


FIGURE 21. System structure diagram of 2-DOF control with set point filter type.

The controller  $C_2(s)$  is

$$C_2(s) = \frac{Q_2(s)}{1 - G_m(s)Q_2(s)} \quad (35)$$

The  $C_2(s)$  can be transformed into the PID controller structure shown in (36):

$$\begin{cases} C_2(s) = \frac{(Ts + 1)^2}{Ks [\lambda_2^2 s + (2\lambda_2 + \tau)]} \\ \quad = K_p \left( 1 + \frac{1}{T_I s} + T_D s \right) \frac{1}{T_F s + 1} \\ K_p = 2T / [K (2\lambda_2 + \tau)] \\ T_I = 2T \\ T_D = T / 2 \\ T_F = \lambda_2^2 / (2\lambda_2 + \tau) \end{cases} \quad (36)$$

Equation (36) can be further improved into the form of incremental PID to ensure that the control quantity changes smoothly when the output weight of each sub-controller is changed. Fig.22 shows the block diagram of 2-DOF-IMC system based on the controller parameter adaptive strategy.

**B. MULTI-MODEL ADAPTIVE STRATEGY**

Single-model control strategies can often only achieve good control results in modeling conditions. After adding controller parameter adaptation, it can improve the adaptability of single-model control strategy to small-scale working condition changes. The multi-model adaptive strategy can improve the system’s adaptability to the full range of working conditions.

This paper adopts a 2-DOF-IMC controller output weighting scheme under typical load conditions to implement a multi-model adaptive strategy. The specific method is the recursive bayesian probability weighting method. The algorithm calculates the weight based on the error between the sub-model and the actual system [39]. The recursive probability calculation equation is:

$$G_{j,k} = \frac{\exp\left(-\frac{1}{2}K(y(k) - \hat{y}_j(k))^2\right) G_{j,k-1}}{\sum_{i=1}^N \left(\exp\left(-\frac{1}{2}K(y(k) - \hat{y}_i(k))^2\right) G_{i,k-1}\right)} \quad (37)$$

In the equation,  $G_{j,k}$  is the recursive bayesian weighted probability of the  $j$ -th model at time  $k$ ;  $y(k)$  is the output value of the system at time  $k$ ;  $\hat{y}_j(k)$  is the predicted value output by the  $j$ -th sub-model at time  $k$ ;  $K$  is the recursive calculation Convergence coefficient;  $N$  is the number of sub-models. The value of the convergence coefficient determines

the rate of convergence to the model with the smallest error. The larger the value, the faster the convergence rate. However, if the value of the convergence coefficient is too large, it may cause the controller to oscillate between different sub-models, which will increase the instability of the system.

It can be seen from (37) that the probability of recurrence is not only related to the error at the current moment, but also related to the historical probability. When it completely converges to a certain model, the probability of the model is 1, and the probability of the other models is 0, and the subsequent recursive process will exclude all the remaining models.

To ensure that all model probabilities are not lost, a smaller number  $\delta$  is set as the small probability cutoff value. That is, when  $G_{j,k} \leq \delta$ , let  $G_{j,k} = \delta$ . The calculation equation for the weight of each sub-controller is:

$$w_{j,k} = \begin{cases} G_{j,k} / \sum_{i=1, i \neq o}^N G_{i,k} & G_{j,k} > \delta \\ 0 & G_{j,k} = \delta \end{cases} \quad (38)$$

In the equation,  $w_{j,k}$  is the weight of the output of the sub-controller corresponding to the sub-model  $j$  at the time  $k$ ;  $o$  is the set of sequence numbers  $j$  that satisfy  $G_{j,k} = \delta$ .

The recursive bayesian probability weighting method converges quickly, has a small amount of calculation, and the switching process is stable. Block diagram of a multi-model adaptive 2-DOF-IMC system is shown in the Fig.23.

**C. IMPLEMENTATION PROCESS OF ADAPTIVE TWO-DEGREE-OF-FREEDOM INTERNAL MODEL CONTROL**

In summary, the implementation process of the adaptive 2-DOF-IMC strategy is:

- 1) Identify the transfer function model of the controlled object under various typical working conditions.
- 2) Using the model obtained by the identification, design the 2-DOF-IMC controller under each typical working condition.
- 3) Use the NSGA-II method based on chaotic mutation to tune the parameters of the 2-DOF-IMC controller in each typical working condition.
- 4) According to the parameter tuning results, the  $T - S$  fuzzy scheduling method is used to design a 2-DOF-IMC controller with adaptive parameters under various typical working conditions.
- 5) The recursive bayesian probability weighting method is used to weight and sum the output of the parameter adaptive 2-DOF-IMC controller under various typical working conditions to obtain a multi-model adaptive 2-DOF-IMC strategy.

**D. SIMULATION TEST AND ANALYSIS**

According to the methods in Sections 4.1~4.3, four control strategies are designed for simulation test. The four strategies are:

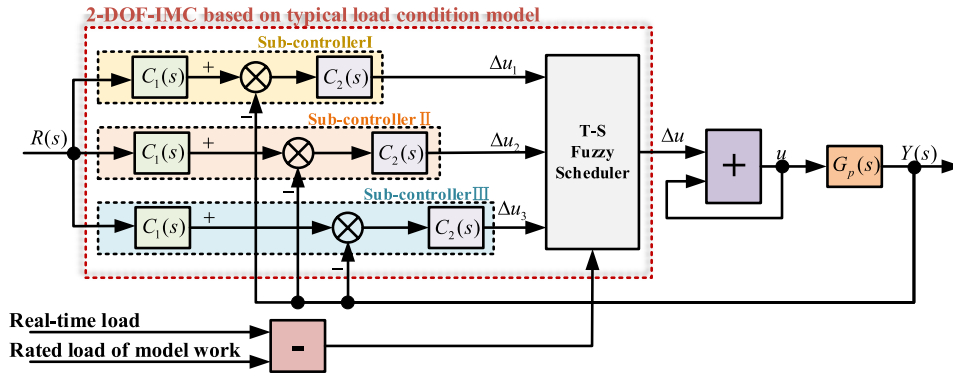


FIGURE 22. Block diagram of a 2-DOF-IMC system based on the controller parameter adaptive strategy.

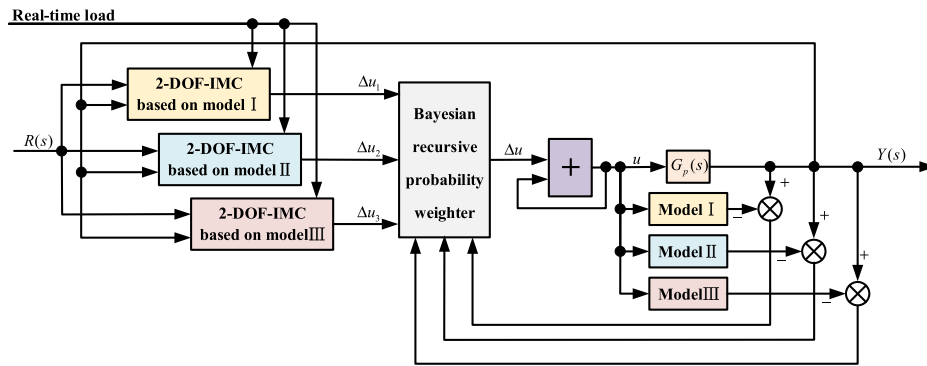


FIGURE 23. Block diagram of a multi-model adaptive 2-DOF-IMC system.

- 1) Single-model 2-DOF-IMC (Denoted as Single-model). This strategy uses the system estimated model to design the controller under 450MW load, and the controller parameters use ParametersIII.
- 2) Single-model and parameter-adaptive 2-DOF-IMC (Denoted as Single-model and parameter-adaptation). This strategy uses the system estimated model to design the controller under 450MW load, and the controller parameters are designed using the adaptive method in 4.1.
- 3) Multi-model 2-DOF-IMC (Denoted as Multi-model). This strategy adopts the system estimated model to design sub-controllers under 350MW, 450MW and 550MW loads and adopts the model adaptive method in 4.2. The parameters of each sub-controller adopt ParametersIII.
- 4) Multi-model and parameter-adaptive 2-DOF-IMC (Denoted as Multi-model and parameter-adaptation). This strategy adopts the system estimated model design sub-controller under 350MW, 450MW, 550MW loads and adopts the model adaptation method in 4.2. The parameters of each sub-controller are designed using the adaptive method in 4.1.

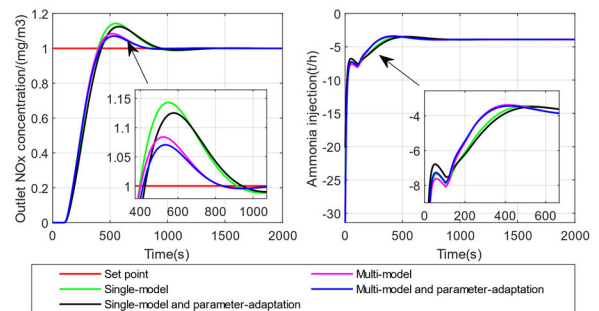


FIGURE 24. Comparison of set point tracking performance of four control strategies under 400MW load condition.

point of  $1\text{mg}/\text{m}^3$ , to investigate the set point tracking ability of the control system. The system response curve and control quantity curve under four control strategies are shown in Fig.24 and Fig.25. The quantitative performance indexes are shown in Table 10, where  $M_p$  is the overshoot of step response,  $T_s$  is the system stability time ( $\pm 0.02$ ),  $MSE$  is the mean square error of the system response, and  $E$  is the mean square control quantity of the system.

Under 400MW load conditions: the time for the four control strategies to reach the set point for the first time is basically the same; The single-model strategy has the largest overshoot and the longest transition time; After adding parameter adaptation to the Single-model strategy, the overshoot has been improved; The Multi-model strategy is

#### 1) COMPARATIVE ANALYSIS OF DYNAMIC PERFORMANCE

Under 400MW and 500MW load conditions, a unit step signal is applied to the SCR denitration system, that is, a set

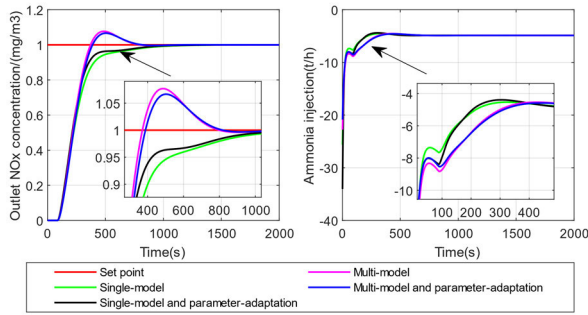


FIGURE 25. Comparison of set point tracking performance of four control strategies under 500MW load condition.

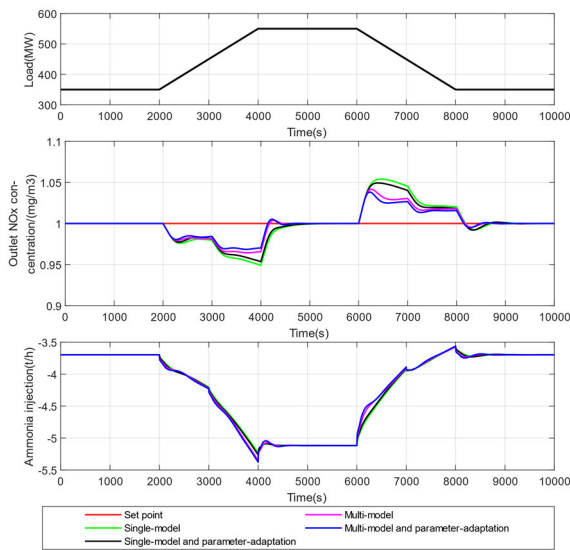


FIGURE 26. Comparison of anti-disturbance performance of 4 control strategies.

significantly better than the Single-model strategy in terms of overshoot and adjustment time; After adding parameter adaptation to the Multi-model strategy, the dynamic performance of the system is further improved.

Under 500MW load conditions: The Single-model strategy is in an underdamped state, and the adjustment is slow; After adding parameter adaptation to the Single-model strategy, the system response speed is slightly improved; Multi-model strategy has fast response speed and small overshoot; After adding parameter adaptation, the overshoot of the Multi-model strategy is further reduced.

## 2) COMPARATIVE ANALYSIS OF ANTI-DISTURBANCE PERFORMANCE

Test the anti-disturbance ability of the system under different control strategies. After the closed-loop control system is adjusted smoothly under the action of the unit step set point, the variable load test will be carried out. Assuming that the initial unit load is 350MW, the unit load increases to 550MW at a rate of 6MW/min at 2000s, and the unit load drops to 350MW at a rate of 6MW/min at 6000s. The comparison of

TABLE 10. Comparison of dynamic performance indexes of four control strategies under atypical conditions.

Load (MW)	Strategy	$M_p$ /%	$T_s$ /s	$MSE / 10^{-2}$	$E$
400	Single-model	14.31	840	10.59	21.84
	Single-model and parameter-adaptation	12.50	859	11.12	20.52
	Multi-model	8.39	730	10.25	22.05
	Multi-model and parameter-adaptation	7.04	725	10.29	21.92
500	Single-model	0	804	9.39	28.36
	Single-model and parameter-adaptation	0	759	8.91	29.96
	Multi-model	7.69	685	9.07	30.03
	Multi-model and parameter-adaptation	6.67	692	9.28	29.42

TABLE 11. Comparison of dynamic performance indexes of four control strategies under atypical conditions.

Strategy	$MSE / 10^{-4}$	$E$
Single-model	5.28	17.914
Single-model and parameter-adaptation	4.34	17.919
Multi-model	2.85	17.924
Multi-model and parameter-adaptation	2.21	17.927

the effect of system anti-disturbance capability is shown in Fig.26. The quantitative performance indexes are shown in Table 11, where  $MSE$  is the mean square error of the system response, and  $E$  is the mean square control quantity of the system.

It can be seen that the anti-disturbance ability of the Multi-model strategy is better than the Single-model strategy. After adding parameter adaptation, the anti-disturbance capabilities of the Multi-model strategy and the Single-model strategy have been enhanced.

## VI. CONCLUSION

This paper takes a 600MW thermal power unit as the research object, and proposes an adaptive 2-DOF-IMC algorithm for the full range control of the SCR denitration system.

The intelligent identification method based on DEQPSO was used to establish the transfer function model of the ammonia injection-SCR outlet  $NO_x$  concentration under 3 typical working conditions. On this basis, three 2-DOF-IMC controllers were established. Taking the set point tracking performance, anti-disturbance performance and control energy consumption of the control system as the objective function, the pareto optimal solution of the controller parameters is obtained by using the NSGA-II algorithm based on chaotic mutation. Aiming at the over-damping or under-damping problems that may occur when the actual working conditions deviate from the rated working conditions of the controller, the  $T - S$  fuzzy scheduler is used to design the controller parameter adaptive strategy. In order to improve the adaptability of the controller to the full range

of working conditions, the recursive Bayesian probability weighting method is used to weight and sum the output of the controller under each typical working condition to obtain a multi-model adaptive strategy.

The test results show that the multi-model adaptive controller is better than the single-model controller in terms of set point tracking and anti-disturbance, which is manifested in a shorter transition time and a smaller overshoot; After adding control parameter adaptation to single-model and multi-model controllers, the control quality of the system can be further improved, which is mainly reflected in the reduction of overshoot; Multi-model adaptation is more adaptable to the full range of working conditions than parameter adaptation.

Based on the existing research results, the future research directions are as follows:

- 1) Explore the model online identification, no disturbance switching scheme, to achieve regular maintenance of the internal model controller model.
- 2) Using machine learning algorithm to soft measure  $NO_x$  concentration at the entrance of SCR system. According to the chemical reaction equation molar ratio to calculate the ammonia injection feedforward.
- 3) Embed the algorithm into the optimized control platform developed by the team.

## REFERENCES

- [1] Y. Zhang, Q. Feng, S. Li, K. Xu, Y. Pei, and Y. Zhu, "Study on operation status of SCR denitration system in Chinese coal-fired power plants," *IOP Conf. Ser. Earth Environ. Sci.*, vol. 467, no. 1, p. 12119, 2020, doi: [10.1088/1755-1315/467/1/012119](https://doi.org/10.1088/1755-1315/467/1/012119).
- [2] L. Yan, Z. Dong, H. Jia, J. Huang, and L. Meng, "Dynamic inferential  $NO_x$  emission prediction model with delay estimation for SCR de- $NO_x$  process in coal-fired power plants," *Roy. Soc. Open Sci.*, vol. 7, no. 2, Feb. 2020, Art. no. 191647, doi: [10.1098/rsos.191647](https://doi.org/10.1098/rsos.191647).
- [3] M.-G. Kim, D.-C. Seo, and H.-T. Chung, "A CFD study on flow control of ammonia injection for denitrification processes of SCR systems in coal-fired power plants," *Energies*, vol. 14, no. 5, p. 1352, Mar. 2021, doi: [10.3390/en14051352](https://doi.org/10.3390/en14051352).
- [4] S. Huang, B. Su, Y. Hua, L. Sun, and J. Wang, "Gas turbine  $NO_x$  emission control technology," *Electr. Power*, vol. 45, no. 6, pp. 100–103, 2012.
- [5] K. Nakamura, T. Muramatsu, T. Ogawa, and T. Nakagaki, "Prediction of de- $NO_x$  performance using monolithic SCR catalyst under load following operation of natural gas-fired combined cycle power plants," *Energy*, vol. 227, Jul. 2021, Art. no. 120383, doi: [10.1016/j.energy.2021.120383](https://doi.org/10.1016/j.energy.2021.120383).
- [6] T. Qin, J. Liu, T. Yang, and W. Zhang, "SCR denitration system modeling and operation optimization simulation for thermal power plant," *Proc. CSEE*, vol. 36, no. 10, pp. 2699–2703, 2016.
- [7] Z. Zhao, Y. Ren, C. Mu, T. Zou, and K.-S. Hong, "Adaptive neural-network-based fault-tolerant control for a flexible string with composite disturbance observer and input constraints," *IEEE Trans. Cybern.*, early access, Jul. 7, 2021, doi: [10.1109/TCYB.2021.3090417](https://doi.org/10.1109/TCYB.2021.3090417).
- [8] Z. Zhao, Z. Liu, W. He, K.-S. Hong, and H.-X. Li, "Boundary adaptive fault-tolerant control for a flexible Timoshenko arm with backlash-like hysteresis," *Automatica*, vol. 130, Aug. 2021, Art. no. 109690, doi: [10.1016/j.automatica.2021.109690](https://doi.org/10.1016/j.automatica.2021.109690).
- [9] Z. Zhao, X. He, Z. Ren, and G. Wen, "Boundary adaptive robust control of a flexible riser system with input nonlinearities," *IEEE Trans. Syst., Man, Cybern., Syst.*, vol. 49, no. 10, pp. 1971–1980, Oct. 2019, doi: [10.1109/TSMC.2018.2882734](https://doi.org/10.1109/TSMC.2018.2882734).
- [10] Z. Zhao, C. K. Ahn, and H.-X. Li, "Dead zone compensation and adaptive vibration control of uncertain spatial flexible riser systems," *IEEE/ASME Trans. Mechatronics*, vol. 25, no. 3, pp. 1398–1408, Jun. 2020, doi: [10.1109/TMECH.2020.2975567](https://doi.org/10.1109/TMECH.2020.2975567).
- [11] X. Yu, W. He, H. Li, and J. Sun, "Adaptive fuzzy full-state and output-feedback control for uncertain robots with output constraint," *IEEE Trans. Syst., Man, Cybern. Syst.*, vol. 51, no. 11, pp. 6994–7007, Nov. 2021, doi: [10.1109/TSMC.2019.2963072](https://doi.org/10.1109/TSMC.2019.2963072).
- [12] L. Kong, W. He, W. Yang, Q. Li, and O. Kaynak, "Fuzzy approximation-based finite-time control for a robot with actuator saturation under time-varying constraints of work space," *IEEE Trans. Cybern.*, vol. 51, no. 10, pp. 4873–4884, Oct. 2021, doi: [10.1109/TCYB.2020.2998837](https://doi.org/10.1109/TCYB.2020.2998837).
- [13] C. Yang, D. Huang, W. He, and L. Cheng, "Neural control of robot manipulators with trajectory tracking constraints and input saturation," *IEEE Trans. Neural Netw. Learn. Syst.*, vol. 32, no. 9, pp. 4231–4242, Sep. 2021, doi: [10.1109/TNNLS.2020.3017202](https://doi.org/10.1109/TNNLS.2020.3017202).
- [14] C. Yang, D. Huang, W. He, and L. Cheng, "Neural control of robot manipulators with trajectory tracking constraints and input saturation," *IEEE Trans. Neural Netw. Learn. Syst.*, vol. 32, no. 9, pp. 4231–4242, Sep. 2021, doi: [10.1109/TNNLS.2020.3017202](https://doi.org/10.1109/TNNLS.2020.3017202).
- [15] G. Liu, Y. Zhang, D. Shen, B. Yuan, R. Li, and Y. Sun, "Anticipatory  $NH_3$  injection control for SCR system based on the prediction of the inlet  $NO_x$  concentration," *J. Energy Inst.*, vol. 94, pp. 167–175, Feb. 2021, doi: [10.1016/j.joei.2020.07.002](https://doi.org/10.1016/j.joei.2020.07.002).
- [16] Y. Tingting, B. Yang, L. You, and Z. Wenguang, "Study on multi-objective optimal control of SCR denitrification system," *Proc. CSEE*, vol. 41, no. 14, pp. 4905–4911, 2021, doi: [10.13334/j.0258-8013.pcsee.201674](https://doi.org/10.13334/j.0258-8013.pcsee.201674).
- [17] D. Ming, N. Yuguang, P. Xiangfeng, C. Guoqing, M. A. Qiang, and Z. Zhibao, "Optimal control of SCR denitrification system based on improved fuzzy linear active disturbance rejection controller," *J. Chin. Soc. Power Eng.*, vol. 41, no. 9, pp. 743–748, 757, 2021, doi: [10.19805/j.cnki.jcspe.2021.09.005](https://doi.org/10.19805/j.cnki.jcspe.2021.09.005).
- [18] X. Huang, Z. Qi, Y. Fan, L. Wang, Y. Zheng, and J. Zhang, "MD-TDOF-PID control of SCR denitration system," *Instrumentation*, vol. 25, no. 9, pp. 18–20, 2018.
- [19] J. Zhang, B. Jia, B. Zou, X. Tian, and C. Liu, "A multiple model control method of coal-fired power plant SCR-De $NO_x$  system," in *Proc. Int. Conf. Intell. Comput. Sustain. Energy Environ.*, in Communications in Computer and Information Science, vol. 925, 2018, doi: [10.1007/978-981-13-2381-2\\_29](https://doi.org/10.1007/978-981-13-2381-2_29).
- [20] Q. Jin, X. Du, Q. Wang, and L. Liu, "Analytical design 2 DOF IMC control based on inverted decoupling for non-square systems with time delay," *Can. J. Chem. Eng.*, vol. 94, no. 7, pp. 1354–1367, Jul. 2016, doi: [10.1002/cjce.22505](https://doi.org/10.1002/cjce.22505).
- [21] J. Zhang, *Two Degrees of Freedom Control*. Electronic Industry Press, 2012.
- [22] K. Nishad, F. Ries, J. Janicka, and A. Sadiki, "Analysis of spray dynamics of urea–water-solution jets in a SCR-De $NO_x$  system: An LES based study," *Int. J. Heat Fluid Flow*, vol. 70, pp. 247–258, Apr. 2018, doi: [10.1016/j.ijheatfluidflow.2018.02.017](https://doi.org/10.1016/j.ijheatfluidflow.2018.02.017).
- [23] X. Huang, "Research on control strategy and application of model-driven PID," Ph.D. dissertation, North China Electr. Power Univ., Beijing, China, 2016.
- [24] J. Wu, Z. Zhang, and X. Liu, "Research on the correlation between the load change of coal-fired power plant units and SCR system parameters," *Environ. Eng.*, no. 8, pp. 131–135, 2021.
- [25] T. Qin, "Modeling of SCR flue gas denitrification system in coal-fired power plant and optimized control of ammonia injection," Ph.D. dissertation, North China Electr. Power Univ., Beijing, China, 2017.
- [26] Y. F. Xu, J. Gao, G. C. Chen, and J. S. Yu, "Quantum particle swarm optimization algorithm," *Appl. Mech. Mater.*, vols. 63–64, pp. 106–110, Jun. 2011.
- [27] W. Deng, J. Xu, Y. Song, and H. Zhao, "Differential evolution algorithm with wavelet basis function and optimal mutation strategy for complex optimization problem," *Appl. Soft Comput.*, vol. 100, Mar. 2021, Art. no. 106724, doi: [10.1016/j.asoc.2020.106724](https://doi.org/10.1016/j.asoc.2020.106724).
- [28] Y. Mousavi, G. Bevan, and I. B. Kucukdemiral, "Fault-tolerant optimal pitch control of wind turbines using dynamic weighted parallel firefly algorithm," *ISA Trans.*, Oct. 2021, doi: [10.1016/j.isatra.2021.10.019](https://doi.org/10.1016/j.isatra.2021.10.019).
- [29] Y. Mousavi, A. Alfi, and I. B. Kucukdemiral, "Enhanced fractional chaotic whale optimization algorithm for parameter identification of isolated wind-diesel power systems," *IEEE Access*, vol. 8, pp. 140862–140875, 2020, doi: [10.1109/ACCESS.2020.3012686](https://doi.org/10.1109/ACCESS.2020.3012686).
- [30] M. Liu, P. Han, and T. Zhang, "Reheat steam temperature system model identification for ultra-supercritical double reheat units," *Comput. Simul.*, vol. 35, no. 5, pp. 91–99, 2018.
- [31] Y. Zhang, P. Han, and X. Zhang, "Design and research on simulation model of limestone-wet flue gas desulfurization absorption tower," *J. Syst. Simul.*, vol. 31, no. 2, pp. 238–247, 2019.
- [32] A. Mitsuhiro and T. Hidefumi, "Two-degree-of-freedom PID controllers," *Int. J. Control Automat. Syst.*, vol. 1, no. 4, pp. 401–411, 2003.



[33] D. Wang, "Research on parameter setting and regulation performance of two-degree-of-freedom internal model PID controller for supply air temperature of constant air volume air conditioning unit," in *Proc. 31st China Process Control Conf. (CPCC)*, 2020.

[34] K. Deb, A. Pratap, S. Agarwal, and T. Meyarivan, "A fast and elitist multiobjective genetic algorithm: NSGA-II," *IEEE Trans. Evol. Comput.*, vol. 6, no. 2, pp. 182–197, Apr. 2002, doi: [10.1109/4235.996017](https://doi.org/10.1109/4235.996017).

[35] Y. Sun, "Improved chaos genetic algorithm and its application in artillery firepower distribution," Ph.D. dissertation, Northeastern Univ., Boston, MA, USA, 2017.

[36] A. Pumariño, J. A. Rodríguez, J. C. Tatjer, and E. Vigil, "Chaotic dynamics for two-dimensional tent maps," *Nonlinearity*, vol. 28, no. 2, pp. 407–434, Feb. 2015.

[37] X. Jiang, V. Gripon, C. Berrou, and M. Rabbat, "Storing sequences in binary tournament-based neural networks," *IEEE Trans. Neural Netw. Learn. Syst.*, vol. 27, no. 5, pp. 913–925, May 2016, doi: [10.1109/TNNLS.2015.2431319](https://doi.org/10.1109/TNNLS.2015.2431319).

[38] W. Pan, L. Ding, F. Huang, and Y. Sun, "Adaptive genetic algorithm based on chaos 'micro variation,'" *Control Decis.*, vol. 36, no. 8, pp. 2042–2048, 2021.

[39] Y. Mu, H. Zhang, H. Ren, and Y. Cai, "Fuzzy adaptive observer-based fault and disturbance reconstructions for T-S fuzzy systems," *IEEE Trans. Circuits Syst. II, Exp. Briefs*, vol. 68, no. 7, pp. 2453–2457, Jul. 2021, doi: [10.1109/TCSII.2021.3049243](https://doi.org/10.1109/TCSII.2021.3049243).

[40] X. Lin and Z. Wang, "Adaptive multi-objective control strategy based on particle swarm optimization algorithm optimized fuzzy rules," *Control Theory Appl.*, vol. 38, no. 6, pp. 842–850, 2021.

[41] J. Kim and S. Moon, "Recursive Bayesian estimation based indoor fire location by fusing rotary UV sensors," in *Proc. IEEE/ASME Int. Conf. Adv. Intell. Mechatronics (AIM)*, Jul. 2020, pp. 528–533.



**YUAN YANG** currently works with Xi'an Thermal Power Research Institute Company Ltd., China. His main research interests include pattern recognition and computer vision (PRCV), machine learning and artificial intelligence (MLAI), and the design and application of distributed control systems.



**BIN WANG** currently works with Xi'an Thermal Power Research Institute Company Ltd., China. His main research interests include new energy power generation system control and optimization, intelligent optimization control theory and application, and distributed new energy power generation system access to microgrid optimization control.



**DAN CAI** currently works with Nanjing NR Electric Company Ltd., China. His main research interests include intelligent optimization control of large units, complex system modeling, simulation and control, advanced control theory and application, fault diagnosis and fault-tolerant control, industrial process integrated automation, fault diagnosis and fault-tolerant control, and industrial process integrated automation.



**BO HU** currently works with Xi'an Thermal Power Research Institute Company Ltd., China. His main research interests include networked control technology and systems, power production process modeling, simulation and optimization control, advanced control theory and application, power plant automation, and information technology and systems.



**CHANG LIU** currently works with Xi'an Thermal Power Research Institute Company Ltd., China. He has long been engaged in scientific research and engineering in the field of automation. His main research interests include thermal power generating unit modeling, simulation and optimization control, thermal power plant energy saving and management, and wind power generating unit fault diagnosis.



**WEIFENG XU** currently works with Nanjing NR Electric Company Ltd., China. His main research interests include industrial process modeling and simulation, the application of intelligent technology in power station modeling, control and fault diagnosis, and new energy system modeling and optimization control.

...